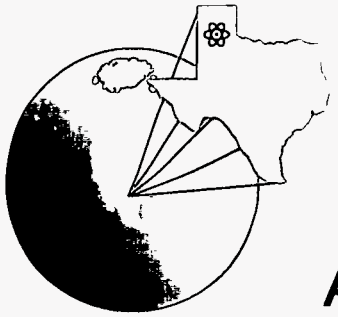

ANRCP-1999-16
April 1999

Amarillo National Resource Center for Plutonium

A Higher Education Consortium of The Texas A&M University System, Texas Tech University, and The University of Texas System

Characterization of Celotex and Thermodynamic Calculations of the Formation of Corrosion Precursors on Beryllium

A. Diaz-Ortiz, J. Stolk, J. Kim, J.M. Sanchez, and A. Manthiram
Materials Science and Engineering Program
The University of Texas at Austin

This report was prepared with the support of the U.S. Department of Energy (DOE), Cooperative Agreement No. DE-FC04-95AL85832. However, any opinions, findings, conclusions, or recommendations expressed herein are those of the author(s) and do not necessarily reflect the views of DOE. This work was conducted through the Amarillo National Resource Center for Plutonium.

Edited by

Angela L. Woods
Technical Editor

600 South Tyler • Suite 800 • Amarillo, TX 79101
(806) 376-5533 • Fax: (806) 376-5561
http://www.pu.org

DISCLAIMER

ANRCP-1999-16

AMARILLO NATIONAL RESOURCE CENTER FOR PLUTONIUM/
A HIGHER EDUCATION CONSORTIUM

A Report on

Characterization of Celotex and Thermodynamic Calculations of the Formation of Corrosion Precursors on Beryllium

A. Díaz-Ortiz, J. Stolk, J. Kim, J. M. Sanchez, and A. Manthiram
Materials Science and Engineering Program
The University of Texas at Austin
Austin, TX 78712

Submitted for publication to

ANRC Nuclear Program

April 1999

CHARACTERIZATION OF CELOTEX AND THERMODYNAMIC CALCULATIONS OF THE FORMATION OF CORROSION PRECURSORS ON BERYLLIUM

A. Díaz-Ortiz, J. Stolk, J. Kim, J. M. Sanchez, and A. Manthiram
Materials Science and Engineering Program

Abstract

A complete compositional and thermal characterization of celotex was carried out using energy dispersive spectroscopy, inductively coupled plasma-mass spectroscopic analysis, ion chromatography, and thermogravimetric analysis. Both fluoride and sulfate anions in addition to chloride as well as several metal ions are found to be present. The chloride present in celotex is lost at moderate temperatures 200<T<400°C, which may have important consequences on the formation of corrosion precursors.

Equilibrium thermodynamic calculations on the stability of beryllium oxide in chlorinated environments were performed for a model system composed by beryllium, carbon, chlorine, hydrogen and oxygen. The calculations were aimed at describing the equilibrium, long-term behavior of a beryllium surface and its interaction with chlorine in a closed environment. We found that (i) carbon is essential for the formation of $BeCl_2$, and (ii) the chlorine-to-hydrogen ratio in chlorinated solvents is an important quantity since for solvents with chlorine-to-hydrogen ratio higher than 1, $BeCl_2$ is not formed independently of the amount of solvent.

TABLE OF CONTENTS

LIST OF TABLES

LIST OF FIGURES

1. INTRODUCTION

The importance of safe and long-term storage of nuclear weapons components has drawn attention towards the characterization and understanding of the corrosion precursors formed on beryllium. Both celotex, which is used as a packing material inside the AL-R8 storage containers, and the chlorinated solvents that are used for degreasing beryllium parts have been evidenced before to be the source of the aggressive anion, chloride, which can cause pitting corrosion on beryllium. An understanding of the corrosion behavior of beryllium in the environment of the storage containers and of the roles played by the various chemical constituents in the degreasing agents is of vital importance.

Recently, several groups have focused on the corrosion of beryllium and the corrosion precursors formed on beryllium surfaces (LeMay, 1995; Hill *et al.*, 1996; Lillard *et al.*, 1997; Birkbeck *et al.*, 1999). Beryllium chloride is soluble in water and it is known to induce corrosion in beryllium metal. Experiments have shown the presence of chloride corrosion precursors on the surfaces of beryllium used in nuclear weapons. There is evidence that the chloride present on the surface of beryllium originate either from the chlorinated solvents such as 1,1,1-trichloroethane (TCA) and 1,1,2-trichloroethylene (TCE) that are used as degreasing agents in the nuclear industry or from the celotex, which is used as a packing material inside the AL-R8 containers.

Despite the prior work on the corrosion behavior of beryllium, the issue of how the interaction of the different organic and inorganic compounds with beryllium ultimately affect the general corrosion of the metal and the stability of the ubiquitous protective oxide layer remains unclear. To address this issue, we have focused on two aspects during the past year: (i) a complete characterization of the chemical composition of celotex and its thermal stability, and (ii) the prediction based on thermodynamic calculations of the reaction products formed by the interaction of beryllium with organic solvents.

2. EXPERIMENTAL AND METHODOLOGY

The compositional characterization of celotex was carried out both by energy dispersive spectroscopic (EDS) analysis in scanning electron microscopy (SEM) and wet-chemical procedures. EDS analysis was carried out at various points with various batches of celotex in order to assess the homogeneity in chemical composition. The wet-chemical procedures utilized inductively coupled plasma-mass spectroscopic (ICPMS) analysis and ion chromotographic (IC) analysis. The solution for the ICPMS analysis was prepared by adding concentrated nitric acid to 0.2 g of celotex and allowing the sample to leach for 48 hours. An aliquot of the solution so obtained was diluted and analyzed for various elements. The IC analysis was carried out with extracts obtained by digesting 2 g of celotex in deionized water for 4 hours at 90°C.

Thermal stability of celotex was assessed both with thermogravimetric analysis (TGA) and differential scanning calorimetry (DSC). TGA and DSC experiments were carried out with a heating rate of, respectively, 2 and 10°C/min.

Thermodynamic calculations were made using Thermo-Calc Software (Sundman *et al.*, 1985, Thermocalc) along with the Scientific Group Thermodata Europe (SGTE) (Ansara and Sundman, 1986) databank. The calculations were performed with a simple model system consisting of a few important elements: beryllium, oxygen, chlorine, carbon, and hydrogen.

Table 1: Energy Dispersive Spectroscopy Characterization of As-Received Celotex Sample S1

Element	Amount, weight percent					
	Area 1	Area 2	Area 3	Area 4	Area 5	Average
Al	13.01	22.01	25.11	17.88	15.08	18.62
Si	36.03	50.45	55.71	49.96	46.36	47.70
S	3.88	4.43	2.80	4.28	4.48	3.97
Cl	3.31	3.88	2.94	4.42	4.57	3.82
K	8.42	4.97	3.75	5.77	7.68	6.12
Ca	13.85	7.52	5.17	9.91	11.25	9.54
Ti	2.59	1.06	0.94	1.69	2.54	1.76
Fe	18.92	5.69	3.59	6.08	8.05	8.47

Table 2: Energy Dispersive Spectroscopy Characterization of As-Received Celotex Sample S2

Element	Amount, weight percent					
	Area 1	Area 2	Area 3	Area 4	Area 5	Average
Al	22.07	21.33	17.75	20.77	19.37	20.26
Si	52.48	49.57	48.13	54.29	50.61	51.02
S	4.52	5.01	5.18	5.32	5.09	5.02
Cl	5.47	6.98	6.25	2.99	3.27	4.99
K	4.53	6.49	6.32	3.57	5.16	5.21
Ca	6.65	6.48	10.41	6.94	9.30	7.96
Ti	1.04	1.05	1.50	1.61	1.65	1.37
Fe	3.24	3.09	4.44	4.52	5.55	4.17

Table 3. Energy Dispersive Spectroscopy Characterization of As-Received Celotex Sample S3

Element	Composition, weight percent					
	Area 1	Area 2	Area 3	Area 4	Area 5	Average
Al	22.70	24.08	31.22	29.01	31.11	27.62
Si	53.27	40.18	49.72	51.98	54.99	50.03
S	3.20	8.30	3.71	1.25	2.37	3.77
Cl	3.43	6.99	2.97	3.45	1.29	3.63
K	4.04	4.44	3.09	3.00	2.68	3.45
Ca	9.10	12.32	5.19	7.73	4.26	7.72
Ti	0.94	0.42	0.59	0.88	0.77	0.72
Fe	3.32	3.27	3.51	2.71	2.52	3.07

3. RESULTS AND DISCUSSION

3.1. Characterization of Celotex

Celotex is a sugarcane bagasse fiber. According to the materials safety data sheet (MSDS), it consists of primarily cellulose (< 95%) and starch (< 9%). In addition to these organic constituents, it consists of trace amounts of inorganic constituents such as clay. Since the inorganic species present in the celotex can play a critical role in forming the corrosion precursors, a qualitative and quantitative determination of the various cations and anions present will be valuable. Accordingly, we used EDS, ICPMS, and IC analyses to determine the inorganic constituents.

Tables 1–3 give the EDS results for three celotex samples—S1, S2 and S3—that were cut from three different places of a bigger celotex packing material. For each sample, the EDS data collected at five different areas and their average are presented in these Tables. It should be noted that the numbers presented in Tables 1–3 are obtained by assuming that the sum of the weight % of all the elements listed in the table corresponds to 100%. Therefore, the actual weight % of these elements in celotex will be much smaller than these numbers since celotex contains only <5% inorganic constituents and the remaining >95% corresponds to organic constituents such as cellulose and starch.

The EDS data show the presence of Al, Si, S, Cl, K, Ca, Ti and Fe. Our EDS analysis has the limitation that it cannot detect lighter elements with atomic number lower than 12. While the qualitative presence of all the elements listed in Tables 1–3 are found consistently in each area and sample of celotex, the quantity of each of these elements vary from one area to another. The observed inhomogeneity and scattering in the contents from one area to another is understandable owing to the fibrous nature of celotex.

Table 4: Inductively Coupled Plasma-Mass Spectroscopic Analysis Data of Celotex (n.d. Means Not Detected).

Element	Amount µg/g	Element	Amount µg/g
Al	5540	Hg	n.d.
Sb	n.d.	Mo	0.434
As	0.263	Nd	0.700
Ba	11.3	Ni	9.08
Be	n.d.	Nb	n.d.
Bi	n.d.	Os	n.d.
B	10.6	Pd	n.d.
Cd	n.d.	Pt	n.d.
Ce	1.49	Pr	0.197
Cs	n.d.	Re	n.d.
Cr	2.03	Rh	n.d.
Co	0.122	Ru	n.d.
Cu	4.22	Sm	n.d.
Dy	n.d.	Se	n.d.
Er	n.d.	Ag	n.d.
Eu	n.d.	Na	896
Gd	n.d.	Ta	n.d.
Ga	0.752	Te	n.d.
Ge	n.d.	Tb	n.d.
Au	n.d.	Tl	n.d.
Hf	n.d.	Th	0.288
Ho	n.d.	Tm	n.d.
Ir	n.d.	Sn	n.d.
Fe	305	Ti	11
La	0.687	W	n.d.
Pb	1.03	U	0.112
Li	0.286	V	1.15
Lu	n.d.	Yb	n.d.
Mg	210	Y	0.432
Mn	9.94	Zn	11.6
		Zr	0.583

Table 5: Ion Chromatography Data of Celotex (n.d. Means Not Detected)

Ion		Amount μg/g
Anions	Fluoride	50
	Chloride	960
	Nitrite	n.d.
	Bromide	9.0
	Nitrate	n.d.
	Phosphate	n.d.
	Sulfate	1600
Cations	Ammonium	n.d.
	Potassium	450
	Calcium	880

Tables 4 and 5 give, respectively, the ICPMS and IC data of celotex. The major elements present (> 1 μg/g of celotex) according to the ICPMS data are Al, Ba, B, Ce, Cr, Cu, Fe, Pb, Mg, Mn, Ni, Na, Ti, V, and Zn. The major anions present according to the IC data are fluoride, chloride, bromide and sulfate. IC analysis also indicates the presence of significant amount of potassium and calcium cations. Previous studies (LeMay, 1995; Lillard *et al.*, 1997) have focused mostly on the amounts of chloride and fluoride extracted from celotex since chloride is known to cause pitting corrosion on beryllium. Our analysis shows the presence of significant amount of sulfate in celotex in addition to chloride and fluoride. In fact the concentration of sulfate found is much higher than that of chloride (Table 5) and the role of the sulfate ions on the corrosion behavior of beryllium needs to be considered. Also, our ICPMS, IC and EDS analyses show the presence of several cations and they may play a critical role in aiding the corrosion process. The role of cations in the corrosion process needs to be assessed as well.

The amounts of chloride (960 μg/g of celotex) and fluoride (50 μg/g of celotex) found in our IC analysis (Table 5) are comparable to those (944 μg of chloride and 125 μg of fluoride per gram of celotex) found by the Lawrence Livermore National Laboratory (LeMay, 1995), but significantly lower than those (1800 μg of chloride and 900 μg of fluoride per gram of celotex) found by the Los Alamos National Laboratory (Lillard *et al.*, 1997). The difference could be due to the shorter time allowed for soaking the celotex in solution in our experiments (4 hours) and Lawrence Livermore Laboratory experiments (2 hours) compared to a longer time (3 weeks) allowed in the Los Alamos National Laboratory experiments. It is possible that the actual amounts of chloride and fluoride in celotex could be

Table 6: Energy Dispersive Spectroscopic Characterization of Celotex Sample S1 after Firing at 400°C

Element	Composition, weight percent					
	Area 1	Area 2	Area 3	Area 4	Area 5	Average
Al	13.46	13.48	13.71	13.96	12.88	13.50
Si	53.53	50.98	55.19	54.21	56.68	54.12
S	4.75	5.31	4.40	4.63	3.69	4.56
K	8.47	9.81	7.77	7.28	7.39	8.14
Ca	10.76	10.69	9.42	10.32	9.39	10.12
Ti	2.24	2.11	2.04	2.26	2.15	2.16
Fe	6.79	7.62	7.46	7.33	7.82	7.40

Table 7: Energy Dispersive Spectroscopic Characterization of Celotex Sample S2 after Firing at 400°C

Element	Composition, weight percent					
	Area 1	Area 2	Area 3	Area 4	Area 5	Average
Al	12.04	12.68	13.17	12.27	13.13	12.66
Si	54.05	55.81	55.62	57.07	48.04	54.12
S	5.45	4.65	4.63	5.12	4.89	4.95
K	7.51	7.41	7.90	6.82	6.78	7.28
Ca	11.39	10.19	9.16	9.80	9.69	10.05
Ti	2.06	2.15	2.45	1.63	2.10	2.08
Fe	7.51	7.10	7.07	7.30	15.37	8.87

Table 8: Energy Dispersive Spectroscopic Characterization of Celotex Sample S3 after Firing at 400°C

Element	Composition, weight percent					
	Area 1	Area 2	Area 3	Area 4	Area 5	Average
Al	14.93	13.68	14.89	13.67	13.00	14.03
Si	51.15	57.54	52.68	52.72	54.71	53.76
S	5.89	4.78	5.28	6.60	6.13	5.74
K	7.74	6.15	7.75	7.05	7.49	7.24
Ca	12.07	9.91	10.37	12.74	10.99	11.22
Ti	1.75	2.03	2.03	1.53	1.90	1.85
Fe	6.47	5.90	7.00	5.70	5.79	6.17

significantly larger than those found by any of these groups as pointed out earlier (Lillard *et al.*, 1997).

Thermogravimetric analysis of celotex in air shows that it begins to decompose around 200°C and the decomposition is complete around 400°C. The decomposition in this temperature range is accompanied by a weight loss of approximately 90%, which corresponds primarily to the loss of carbon and hydrogen as, respectively, CO_2 and H_2O. Differential scanning calorimetry shows a broad exotherm in the temperature range 200–400°C corresponding to the decomposition. Each of the three samples of celotex (S1, S2 and S3 listed in Tables 1–3) showed similar behavior in the TGA and DSC experiments.

EDS analysis was carried out on the residues obtained after firing the three celotex samples (S1, S2 and S3) in air at 400°C for four hours in order to assess whether any other inorganic species is also lost in addition to carbon and hydrogen during the firing process. The EDS analysis data collected at five different areas and their average are given in Tables 6–8. The numbers presented in these Tables 6–8 are obtained by assuming that the sum of the weight % of all the elements listed in the Tables corresponds to 100%.

The residues (approximately 10 weight %) obtained after firing show the presence of all elements that were present in the as-received celotex (Tables 1–3) with the exception of Cl. This indicates that the Cl present in the as-received celotex volatilizes on firing. This observation may possibly suggest the presence of organic chlorides rather than inorganic chlorides in celotex. Further experiments are necessary to identify the nature of the chloride species. The volatilization of Cl on firing also

suggests that the increase in temperature within the storage container may enhance the release of Cl from celotex, which may have important consequences in the corrosion process. The data in Tables 6–8 reveal that the quantity of each of the elements does not vary from one area to another in the residue unlike in the as-received celotex (Tables 1–3). This is due to a more homogeneous nature of the fired powder residue compared to the fibrous nature of the as-received celotex.

3.2 Thermodynamic Predictions Of Corrosion Precursors

Recently, Moddeman and coworkers (Moddeman *et al.*, 1997; Birkbeck *et al.*, 1999), have shown that beryllium chloride is readily formed when the beryllium oxide layer is removed in a chlorinated environment, i.e., scratching or polishing a beryllium sample under a chlorinated solvent. This can be understood on the basis of equilibrium thermodynamics since the reaction $Be+Cl_2 \rightarrow BeCl_2$ is accompanied by high enthalpy of formation (–496 kJ/mol at 300 K).

Under ambient conditions beryllium forms a stable, protective oxide layer on the surface (White and Burke, 1955). The reaction $Be+\frac{1}{2}O_2 \rightarrow BeO$ occurs with an enthalpy of formation of –609 kJ/mol at 300 K. The production of surface chlorides can be investigated by analyzing the stability of this oxide layer in a chlorinated environment. To that aim we selected a model system containing beryllium, carbon, chlorine, hydrogen and oxygen. Once the temperature and the pressure are fixed, the equilibrium state is determined by the minimization of the free energy functional in a five-dimensional space. The minimization was performed using Thermo-Calc (Sundman *et al.*, 1985; Thermocalc) along with the SGTE database (Ansara and Sundman, 1986). All of our calculations were performed at 300 K and 1 atm of pressure.

Our calculations show that carbon plays an important role in the formation of $BeCl_2$ from BeO. This is illustrated in Figure 1 in which the molar fractions of the condensed and the gas phases are plotted against the concentration of carbon in the system. In Figure 1, the amount of each element is fixed with the exception of carbon. From Figure 1 we see that $BeCl_2$ is not formed when the carbon concentration is low. The formation of $BeCl_2$ becomes possible only when the amount of carbon reaches a critical value. The production of CO_2 proceeds as we increase the content of carbon in the system since the reaction $C+O_2 \rightarrow CO_2$ occurs with negative enthalpy of formation (–394 kJ/mol at room temperature). The increase in the mole fraction of the gas phase in Figure 1 is due to the production of CO_2 as carbon is added.

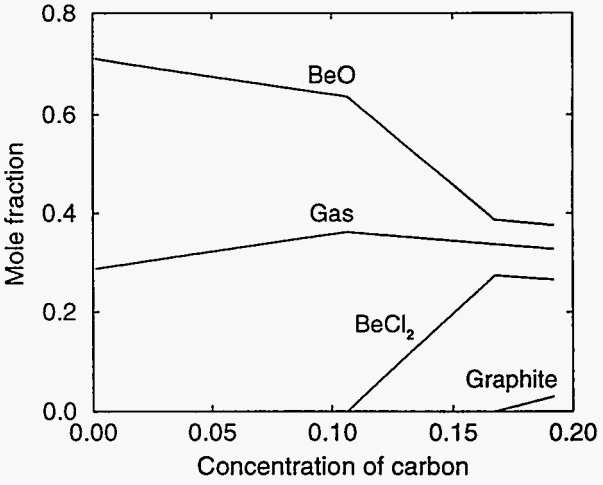

Figure 1: Evolution of the Condensed and Gas Phases of Model System Made of Beryllium, Carbon, Oxygen, Hydrogen And Chlorine, as the Concentration Of Carbon is Varied. [The content of hydrogen in the system is such that the $N(H_2)/N(Cl_2)$ ratio has the value 0.01. The amount of chlorine in the system is $N(Cl_2)/N^*(O_2)=7/15$. See the text for details.]

For low hydrogen concentration, as is the case of Figure 1, we can continue to increase the amount of carbon in the system without producing $BeCl_2$ until all the oxygen in the gas is in the form of CO_2. A further increment in the carbon content still produces CO_2, but in this case BeO provides the oxygen. The formation of CO_2 from BeO allows the production of $BeCl_2$. The mole fraction of $BeCl_2$ increases linearly with the addition of carbon until nearly all the chlorine in the system is in the form of $BeCl_2$. If the concentration of H_2 is large enough, H_2O may be formed. This does not change the mechanism behind the formation of $BeCl_2$, although the equilibrium between the different phases becomes more complicated. We will return to this point later in the report.

The foregoing process is ruled by the presence of carbon and by its abundance respect to oxygen in the gas phase. This suggests that the natural variable to be used to describe the evolution of the BeO phase with the addition of carbon is the ratio of carbon to the initial amount of oxygen in the gas phase, $N(C)/N^*(O_2)$. The $N(C)/N^*(O_2)$ ratio has the value of 1 at the point in which all the oxygen in the gas has been consumed—the onset of the production of $BeCl_2$. In Figure 2 we illustrate this point by plotting the amount of the different phases (normalized to the content of the BeO) against $N(C)/N^*(O_2)$.

From this figure it is apparent that the BeO phase remains unaltered until all the oxygen in the gas is combined with carbon. Figure 2 also illustrates that formation of $BeCl_2$ from BeO is limited by the content of chlorine in the system. Moreover, CO_2 cannot be produced indefinitely as carbon is increased since a Be-pure phase represents a considerable increment in free energy. In other words, it is preferable to maintain the very stable BeO phase and form graphite with the additional carbon.

The relative abundance of the main constituents in the gas phase of Figure 2 (or Figure 1) is shown in Figure 3.

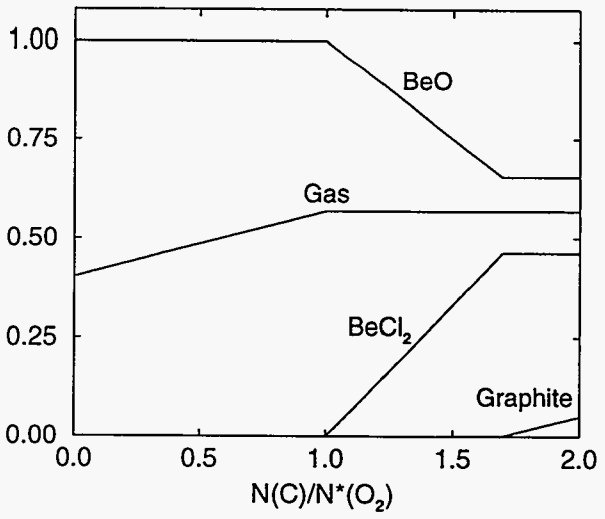

Figure 2: Same Data as in Figure 1 but in This Case the Content of Each of the Phases Have Been Normalized to the Initial Amount of BeO. [The variable $N(C)/N^*(O_2)$ has the value of 1 at the onset of formation of $BeCl_2$.]

This figure illustrates that the formation of CO_2 increases monotonically with the addition of carbon until almost all the chlorine is in the form of $BeCl_2$—small quantities of HCl are formed since the content of H_2 is very low, but finite. Chlorine and oxygen are the major constituents in the gas phase at low concentration of carbon. This implies that at higher concentration of hydrogen, H_2O and HCl molecules can be formed since at room temperature the reactions $2H_2+O_2 \rightarrow 2H_2O$ and $H_2+Cl_2 \rightarrow 2HCl$ occur with enthalpies of −286 kJ/mol and −92 kJ/mol, respectively.

At low concentrations of H_2, water molecules are formed with the oxygen in the gas phase that is not in the form of CO_2 as the reaction $C+O_2 \rightarrow CO_2$ occurs with a higher enthalpy (−394 kJ/mol). On the other hand, at high hydrogen concentration the formation of H_2O and HCl is preferred over the production of CO_2. The formation of large quantities of H_2O and HCl as compared to the amount of CO_2 lowers the free energy.

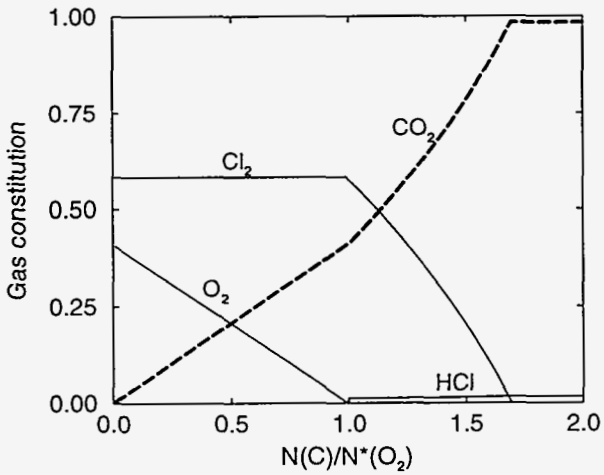

Figure 3: Constitution of the Gas Phase Corresponding to the Data of Figure 2. Water vapor is present in very small quantities and is not shown.

Consequently, the formation of $BeCl_2$ depends on the carbon and hydrogen content.

Figure 4 shows the evolution of the condensed [Figure 4(a)] and gas [Figure 4(b)] phases as a function of the hydrogen content for a value of $N(C)/N^*(O_2)$ ratio equals to 1.35, that is, in the carbon range for which $BeCl_2$ is stable (*cf.* Figure 2). The ratio of hydrogen to chlorine, $N(H_2)/N(Cl_2)$, is the natural variable since the production of HCl limits the production of $BeCl_2$ as we increase the content of H_2 [see Figure 4(b)]. The $N(H_2)/N(Cl_2)$ ratio has the value of 1 at the onset of the formation of $BeCl_2$. From Figure 4(a) we can see that the amount of gas phase increases steadily with the addition of hydrogen reaching a maximum and then decreasing. The decrease in the amount of the gas phase at higher hydrogen concentration is related to the condensation of H_2O molecules and to the formation of graphite, thus diminishing the amount of CO_2 [see Figure 4(b)].

The interplay between carbon and hydrogen on the thermodynamic equilibrium of our model system can be displayed in a general way by plotting the stable phases in the systems as a function of the ratios $N(C)/N^*(O_2)$ and $N(H_2)/N(Cl_2)$. Figure 5 shows the evolution of the different phases in the system as we vary the $N(C)/N^*(O_2)$ and $N(H_2)/N(Cl_2)$ ratios. The phase diagram of Figure 5 also summarizes our previous results since Figures 2 and 4(a) represent cross-sections of Figure 5 at $N(H_2)/N(Cl_2)=0.01$ and $N(C)/N^*(O_2)=1.35$, respectively. Only condensed phases are represented in Figure 5. The hatched region in Figure 5 stands for the BeO phase while the region labeled by $BeO+H_2O$ (l) represents the values of the $N(C)/N^*(O_2)$ and $N(H_2)/N(Cl_2)$ ratios for which BeO and liquid water are the only stable condensed phases. The same labeling procedure holds for the rest of the different regions in Figure 5.

Although we can draw a definite scale in the $N(H_2)/N(Cl_2)$ axis, it is not possible to do the same in the $N(C)/N^*(O_2)$ axis. For values of the $N(H_2)/N(Cl_2)$ ratio less than 1, the onset of the formation of $BeCl_2$ is given by $N(C)/N^*(O_2)=1$, a condition that is independent of the content of chlorine in the system. However, the extent of region $BeO+BeCl_2$ is determined by the concentration of chlorine. At zero content of hydrogen, the boundary between $BeO+BeCl_2+C$ (graphite) and $BeO+BeCl_2$ is given by the condition $N(C)/N^*(O_2)=1+N(Cl_2)/2N^*(O_2)$ (point *f* in Figure 5).

The oxide phase is stable all over the diagram with the exception of the regions that contain $BeCl_2$ as a stable phase. The hydrogen and carbon content in the system, as we mention before, control the formation of $BeCl_2$. For $N(H_2)/N(Cl_2)<1$, the production of $BeCl_2$ starts at $N(C)/N^*(O_2)=1$ and increases linearly with the addition of carbon reaching a maximum at the boundary between the $BeO+BeCl_2$ and $BeO+BeCl_2+C$ regions (*cf.* Figure 2).

On the other hand, for $N(C)/N^*(O_2)>1$, $BeCl_2$ begins to be formed at $N(H_2)/N(Cl_2)=1$ and increases linearly when decreasing the amount of hydrogen in the system [*cf.* Figure

4(a)] attaining a maximum at the boundary between the $BeO+BeCl_2$ and $BeO+BeCl_2+C$ regions. The phase diagram of Fig. 5 can be better understood by noting that along each line defining the boundary between different regions, one phase becomes unstable. For example, along the line passing through points *f* and *g* in Figure 5, the amount of graphite is zero.

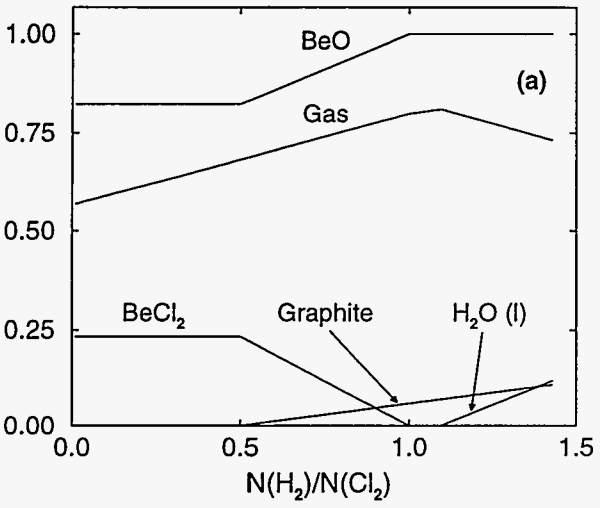

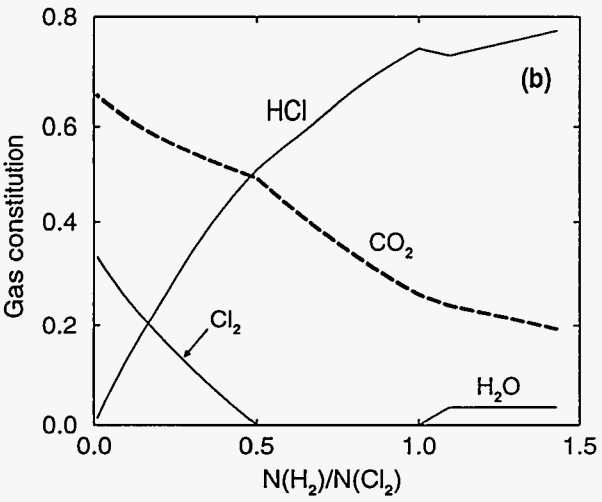

Figure 4: Variation of the Condensed and Gas Phases in the System as the Content of Hydrogen is Varied. The $N(C)/N^*(O_2)$ ratio is 1.35 for which the $BeCl_2$ is a stable phase. In (a) the content of each of the phases is normalized to the initial amount of BeO. As HCl limits the production of $BeCl_2$ the natural variable is $N(H_2)/N(Cl_2)$ ratio instead of $N(H_2)$. In (b) the constitution of the gas phase is shown as a function of the hydrogen-to-chlorine ratio. Compounds present in proportions lower than 10^{-3} are not shown.

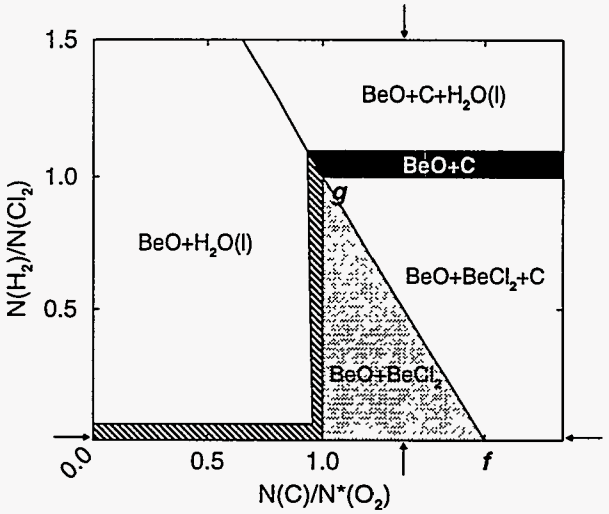

Figure 5: Dependence of the Condensed Phases with the Hydrogen and carbon Contents. BeO is the only stable condensed phase in the hatched region. The horizontal (or vertical) arrows show the path along Figures 2 and 3 (or Figure 4). See text for details.

The phase diagram in Figure 5 depends only on the carbon-to-oxygen, carbon-to-chlorine, and hydrogen-to-chlorine ratios. These ratios are defined by the experimental conditions and by the selection of the solvent. The content of oxygen and hydrogen are variables that can be controlled in the laboratory, while the content of chlorine and carbon can be set by the selection of the solvent. Each point in Figure 5 represents different atmospheric conditions and/or different solvents. For environments containing hydrogen and oxygen in the atmosphere, for example, atmospheric moisture, chlorinated (organic) solvents with a hydrogen-to-chlorine ratio higher than 1, are represented in Figure 5 by points belonging to the $BeO+H_2O$ (l) or BeO+C or $BeO+H_2O$(l)+C regions. Consider, for example, solvents with hydrogen-to-chlorine ratio higher than 1 (such as 1,1,1-trichloroethane). The phase diagram in Figure 5 predicts that under equilibrium conditions $BeCl_2$ does not form independently of the $N(C)/N^*(O_2)$ ratio. On the other hand, if we

consider a solvent with a hydrogen-to-chlorine ratio equal to zero, such as carbon tetrachloride (CCl_4), the formation of $BeCl_2$ is thermodynamically favorable only when $N(C)/N^*(O_2)>1$. Thus, assuming that all carbon in the system is coming from CCl_4, the corrosion precursor $BeCl_2$ will not form if the oxygen content in the gas phase is sufficiently high. However, $BeCl_2$ will form if the oxygen in the gas phase falls above a critical value such as $N(C)/N^*(O_2)>1$.

The importance of the carbon-controlled $BeCl_2$ production is evident since the vapor degreasing with an organic solvent such as 1,1,1-trichloroethane (TCA) or 1,1,2-trichloroethylene (TCE) is the standard procedure for cleaning weapon components. The importance of the hydrogen-to-chlorine ratio in the solvent, on the other hand, is apparent if we compare TCA and TCE. Since TCA has a hydrogen-to-chlorine ratio equal to 1, the equilibrium results predict that $BeCl_2$ is not formed in a hydrogen-containing atmosphere independently of the amount of solvent in the system. In contrast, TCE has a hydrogen-to-chlorine ratio less than 1 and consequently $BeCl_2$ can be formed when the amount of solvent in the system is enough to satisfy the condition $N(C)/N^*(O_2)>1$. The thermodynamic results for TCA and TCE are in qualitative agreement with experiments on these solvents. Birkbeck *et al.*, (1999), examined the effects of residual chlorinated solvents on beryllium on near-ambient conditions by using x-ray photoelectron spectroscopy. After exposing beryllium metal to vapor degreasing with TCA and TCE, Birkbeck and coworkers, found that both solvents leave the beryllium surface chlorinated, with TCE leaving behind a significantly larger chloride concentration that TCA (Birkbeck *et al.*, 1999).

An important feature of high-hydrogen content solvents is that the formation of $BeCl_2$ is prevented by the formation of HCl [*cf.*, Figure 4(b)]. We note, however, that HCl itself may play an important role in the corrosion of beryllium in closed environments, such as the AL-R8 containers. Although the equilibrium thermodynamics results show that HCl does not affect the stability of the BeO phase, kinetic factors should be considered in order to establish the role played by HCl.

Finally, we note that the main changes in the phase diagram of Figure 5 (calculated at 300 K) with temperature relate to the amount of water (liquid) in the system, i.e., at higher temperatures the amount of condensed water is less. The calculated phase diagram is expected to provide a valuable guide to select degreasing solvents, which can avoid or suppress the formation of the corrosion precursor beryllium chloride.

4. CONCLUSIONS

The compositional characterization of celotex reveals the presence of fluoride, chloride and sulfate anions and other elements such as B, Na, Mg, Al, Si, K, Ti, Mn, Fe, Ni, Zn and Ba. Celotex decomposes in the temperature range 200–400°C, losing the organic constituents and Cl. The loss of chlorine at moderate temperatures may have important consequences on the release of chlorine and the formation of the corrosion precursor. The future work is aimed to focus on the release of chlorine as a function of temperature and humidity conditions. Also, the role of sulfate anions that is present in significant amounts in celotex need to be assessed on the corrosion behavior of beryllium.

Thermodynamic calculations have been performed to identify the conditions under which the formation of the corrosion precursor, beryllium chloride, is favored on the surface of beryllium. The calculations show the presence of a threshold amount of carbon and H/Cl ratio < 1 is critical in stabilizing beryllium chloride. Our thermodynamic results for TCA and TCE are in qualitative agreement with the observations of Birkbeck *et al.*, (1999). The calculations may be used as a guide in choosing appropriate solvents for degreasing. However, the kinetics of formation of the precursors is not taken into account in the calculations. The kinetic factors may play a significant role as well.

REFERENCES

1. Ansara, I. and B. Sundman, "The Scientific Group Thermodata Europe," *Computer Handeling and Dissemination Data*, edited by P.S. Glaser (Elsevier Science Publishers, CODATA, 1986).

2. Birkbeck, J.C., N.L. Kuehler, and W.E. Moddeman, *Journal of Surface and Interface Analysis*, to be published (1999).

3. Hill, M.A., D.P. Butt, and R.S. Lillard, "The corrosion/electrochemistry of beryllium and beryllium weldments in aqueous chloride environments," Internal Report, LALN (1996).

4. Lillard, R.S., M.A. Hill, and D.P. Butt, "Preliminary Investigation into the Corrosion of Beryllium Exposed to Celotex and Water," LANL Internal Report, February 1997.

5. LeMay, J.D., "Extraction Analysis of Celotex Packing Material," LLNL, April 1995.

6. Moddeman, W.E., J.C. Birkbeck, and K.C. Coleman, "Chlorides observed on clad metal beryllium," Beryllium Corrosion Meeting Report, LALN, March 1997.

7. Sundman, B., B. Jansson, and J.-O. Andersson, "The Thermo-Calc Databank System," *Calphad* **9** (2), 153 (1985).

8. Thermo-Calc group, Department of Materials Science, Division of Physical Metallurgy, The Royal Institute of Technology, S-100 44 Stockholm, Sweden.

9. White, D.W. and J.E. Burke, eds., *The Metal Beryllium* (American Society of Metals, Cleveland, 1955).